

Positron cooling and annihilation in noble gases

D. G. Green*

Centre for Theoretical Atomic, Molecular and Optical Physics, School of Mathematics and Physics,
Queen's University Belfast, Belfast, BT7 1NN, Northern Ireland, United Kingdom

(Dated: July 1, 2022)

Understanding the dynamics of positron cooling in gases, including the fraction of positrons surviving to thermalisation, is critical for accurate interpretation of positron lifetime spectra, for the development of efficient positron cooling in traps and accumulators, and for a cryogenically cooled, ultra-high-energy-resolution, trap-based positron beam. Here, positron cooling and annihilation in noble gases is simulated using accurate scattering and annihilation cross sections calculated *ab initio* with many-body theory. It is shown that a strikingly small fraction of positrons survive to thermalization: ~ 0.1 in He, ~ 0 in Ne (due to cooling effectively stalling in the relatively deep momentum-transfer cross-section minimum), ~ 0.15 in Ar, ~ 0.05 in Kr and ~ 0.01 in Xe. For Xe, the time-varying annihilation rate $\bar{Z}_{\text{eff}}(\tau)$ is shown to be highly sensitive to the depletion of the distribution due to annihilation, conclusively explaining the long-standing discrepancy between gas-cell and trap-based measurements in Xe. Overall, the use of the accurate atomic data gives $\bar{Z}_{\text{eff}}(\tau)$ in close agreement with experiment for all noble gases except Ne, the experiment for which is proffered to have suffered from incomplete knowledge of the fraction of positrons surviving to thermalization and/or the presence of impurities.

Positrons, the antiparticles of electrons, have important use in e.g., diagnostics of industrially important materials [1–3], in medical imaging in PET (Positron Emission Tomography) scans [4], and in understanding of the composition of the interstellar medium [5]. Interactions of positrons and more complicated antimatter (e.g., anti-hydrogen) with atomic systems are under intense investigation to illuminate collision phenomena [6], perform precision tests of the standard model and gravity [7–9], and to measure rotational excitation and vibrational multimode excitation in molecules [10].

Positrons are typically produced in the laboratory at high energy (e.g., ~ 0.5 MeV for traditional ^{22}Na sources, and ~ 1 keV for nuclear reactor sources, e.g., the NEPO-MUC reactor [3]). As they propagate through a gas of atoms or molecules they lose energy rapidly through ionization, electronic and rotational excitation, and inelastic processes such as molecular dissociation and positronium formation. At energies below the positronium-formation threshold, energy loss in atomic gases proceeds only via

momentum transfer in elastic collisions. Positron annihilation cross sections are typically orders of magnitude smaller than elastic or momentum transfer ones [11], thus positrons tend to undergo many collisions before reaching their inevitable fate of annihilation. Positron cooling dynamics therefore reflect, and thus provide an important probe of, the (complicated) atomic physics of the positron-atom system.

Indeed, observation of lifetime spectra for positrons annihilating in gases was one of the first sources of information on positron interaction with atoms and molecules (see e.g., [12], [13–16] and [17, 18] for reviews). In particular, measurements of the time-varying normalised annihilation rate $\bar{Z}_{\text{eff}}(t)$ during positron thermalization provided information on the energy dependence of the scattering and annihilation cross sections. Understanding the dynamics of positron cooling, including the fraction of positrons surviving to thermalization, is critical for accurate interpretation of the positron lifetime experiments. Incomplete thermalization was suspected to be responsible for the lack of consensus among the \bar{Z}_{eff} data in Xe [19], while modelling of $\bar{Z}_{\text{eff}}(t)$ [20, 21] revealed deficiencies in the theoretical data for neon and the heavier noble-gas atoms. Understanding of positron kinetics is also crucial for the development of efficient positron cooling in traps and accumulators [22], important for e.g., antihydrogen experiments, and for a cryogenically cooled, ultra-high-energy-resolution, trap-based positron beam [23, 24], which can enable the study of positron-induced intramolecular vibrational redistribution and state-resolved measurements of rotational excitation and vibrational multimode excitation in molecules [25]. Developing understanding of cooling dynamics of particles undergoing quantum collisions is also of more general current interest, e.g., for producing ultracold molecules, which hold promise for quantum simulation and for controlled quantum chemistry, via sympathetic cooling with pre-cooled ultracold atoms [26, 27].

Despite the importance of long-standing positron-cooling experimental results [17, 18], there has been a paucity of theoretical studies of positron cooling in gases. Previous studies have mainly employed the diffusion or Fokker-Planck (FP) equation [20, 21, 28–31]. They used semi-empirical or model cross sections, e.g., calculated in the polarised-orbital approximation [32–36], which makes a number of drastic assumptions (e.g., regarding the positron as an infinitely massive particle) and yielded limited success in describing the experiments.

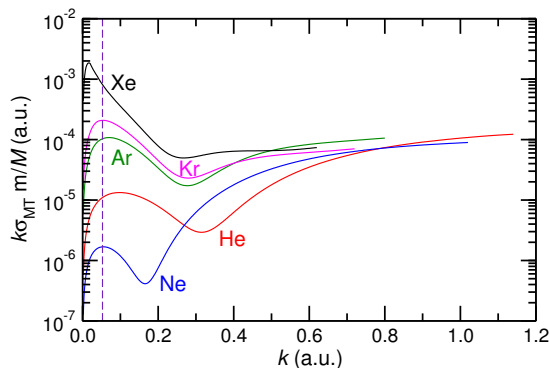


FIG. 1. The mean-squared momentum-transfer coefficient $B(k)/k_{\text{B}}T = k\sigma_{\text{t}}(k)m/M$. Thermal positron momentum $k_{\text{th}} = \sqrt{3k_{\text{B}}T} \sim 0.0528$ a.u. at $T = 293$ K (vertical dashed line).

Positron scattering and annihilation in many-electron systems is characterised by strong positron-atom and electron-positron correlations, e.g., virtual-positronium formation [11, 37–39]. They modify the scattering process, and lead to dramatic enhancements of positron annihilation rates in heavier noble-gas atoms, compared with the single-particle approximation, and influence the shapes of the γ -ray spectra [11, 37–43]. They also make the theoretical description of the positron-atom system a challenging many-body problem.

Recently, many-body theory (MBT) was used to provide an accurate and essentially complete description of low-energy positron interactions with noble-gas atoms, taking full account, *ab initio*, of the strong positron-atom and electron-positron correlations, including virtual-positronium formation. It yielded excellent agreement between theory and experiment for the scattering cross sections, annihilation rates [39, 40], and γ -spectra [39], firmly establishing the relative contributions of annihilation on various atomic orbitals [44].

Here, we show that the MBT data enables accurate modeling of positron cooling and annihilation in noble gases. Using the MBT data in Monte-Carlo (MC) simulations [45, 46], we calculate the time-evolving positron momentum distribution $f(k, \tau)$ [we work in units where τ is the time (in ns) scaled by the number density of the gas n_{g} (in amagat): $\tau = n_{\text{g}}t$] and from this the time-varying annihilation rate $Z_{\text{eff}}(\tau) = \int Z_{\text{eff}}(k)f(k, \tau)dk / \int f(k, \tau)dk$, which can be compared with experiments. The fraction of positrons surviving to thermalisation is shown to be strikingly small. $Z_{\text{eff}}(\tau)$ is shown to be sensitive to the amount of particles annihilating before thermalization, conclusively explaining the long-standing discrepancy between the gas-cell and trap-based Z_{eff} results in Xe. Overall, the MBT-based MC calculations give the best agreement with experiment for all the noble gases to date.

RESULTS

Theory of positron cooling and annihilation

At energies below the positronium-formation threshold, energy loss in atomic gases proceeds only via elastic collisions through momentum transfer. Let $q = p - p'$ denote the momentum transfer in a collision in which the initial and final momenta of the positron have magnitudes p and p' . In a Maxwellian gas of temperature T , the average squared momentum transfer per unit time-density is $\langle q^2/\delta\tau \rangle = 2B(k)$, where $B(k) \equiv k\sigma_{\text{t}}(k)k_{\text{B}}Tm/M$ [47], k and m are the positron momentum and mass, M is the mass of the gas atom and σ_{t} is the positron-atom momentum-transfer cross section. It is calculated as $\sigma_{\text{t}} = 4\pi k^{-2} \sum_{\ell=0}^{\infty} (\ell+1) \sin^2(\delta_{\ell} - \delta_{\ell+1})$ [48], where $\delta_{\ell}(k)$ is the scattering phase shift for a positron of angular momentum ℓ (see [40] for the MBT calculation of δ_{ℓ}). $B(k)$ exhibits a minimum for all atoms in the sequence He–Xe (see Fig. 1), which becomes less pronounced as one moves through the sequence (with the exception of Ne, which has the deepest minimum). As we will see, this leads to “trapping” of positrons and slows down the cooling process in this momentum range.

The annihilation cross section in many-electron targets of number density n_{g} is parametrised as [49, 50],

$$\sigma_{\text{a}} = \pi r_0^2 n_{\text{g}} \frac{c}{v_r} Z_{\text{eff}}, \quad (1)$$

where r_0 is the classical electron radius, c is the speed of light, v_r is the positron speed relative to the target, and Z_{eff} is the dimensionless *effective number of electrons* that contribute to the annihilation process. It is the effective electron density at the positron

$$Z_{\text{eff}} = \int \sum_{i=1}^Z |\Psi_{\mathbf{k}}(\mathbf{r}_1, \dots, \mathbf{r}_Z; \mathbf{r})|^2 \delta(\mathbf{r} - \mathbf{r}_i) d\mathbf{r}_1 \cdots d\mathbf{r}_Z d\mathbf{r}, \quad (2)$$

where \mathbf{r} is the coordinate of the positron of momentum \mathbf{k} , and $\{\mathbf{r}_1, \dots, \mathbf{r}_Z\}$ the coordinates of the Z electrons. Positron-atom and positron-electron correlations can result in $Z_{\text{eff}} \gg Z$ [37, 38, 40]. $Z_{\text{eff}}(k)$ has been calculated recently for the noble gases via diagrammatic MBT, taking full account of correlations (see [40, 51] and ‘Methods’ for a brief review).

From He to Xe, Z_{eff} becomes increasingly large and strongly peaked at low momenta (see Fig. 2). This effect is due to the existence of positron-atom virtual levels [52], signified by large scattering lengths for Ar, Kr and Xe (see Table I in [40]).

Simulations of positron cooling and annihilation

The time-evolving momentum distribution $f(k, \tau)$ is determined via Monte-Carlo simulations based on the ac-

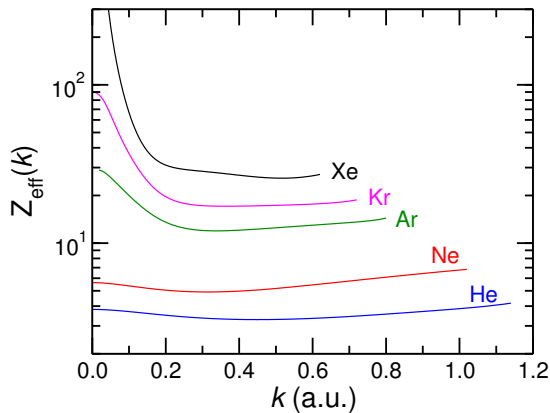


FIG. 2. $Z_{\text{eff}}(k)$ vs positron momentum k calculated using MBT including s, p and d-wave positrons annihilating on valence n and inner valence $(n-1)$ subshells of the noble gases.

curate MBT calculated scattering and annihilation cross sections (see ‘Methods’ for details of the Monte-Carlo algorithm).

Figure 3 is an example of $f(k, \tau)$, calculated for Ar for 50,000 positrons initially distributed uniformly in energy up to positronium-formation threshold [53]. The initial distribution is seen to quickly evolve ($\lesssim 100$ ns amag) to a strong Gaussian-like peak near the minimum in $B(k)$, $k_q^{\text{min}} \sim 0.3$ a.u. (for Ar), which then evolves rather slowly, producing the knee-like feature in the figure. This bunching effect becomes less effective as one moves through the sequence from He–Xe since the minimum in q becomes less pronounced (with the exception of Neon, which has the deepest minimum). However, even in Xe the formation of a peak in $f(k, \tau)$ at small time-densities is still evident. Since for any realistic initial distribution most positrons will have initial momenta $k > k_q^{\text{min}}$, such bunching should be expected, making the overall cooling times somewhat insensitive to the exact form of the initial distribution (see below for further details). The small number of positrons with initial momenta below the minimum at early times cool to thermal energies relatively unimpeded, and they form a second, much smaller peak around thermal momentum $k_{\text{th}} \sim \sqrt{3k_{\text{B}}T} \sim 0.0528$ a.u. As the time-density increases, the Gaussian-like part of the distribution traverses the minimum, roughly maintaining its form as it does so. As more positrons cool below the minimum, the two peaks in the distribution merge, eventually evolving towards the Maxwell-Boltzmann distribution.

As seen in Fig. 3, a strikingly small fraction of positrons survive annihilation before the distribution thermalises. This is true for all the noble gases (see Fig. 4) and has important consequences for the interpretation of measured lifetime spectra (see below). We define the ‘complete’ thermalization time τ_{th} as the time-density at which the r.m.s. momentum of the distribution

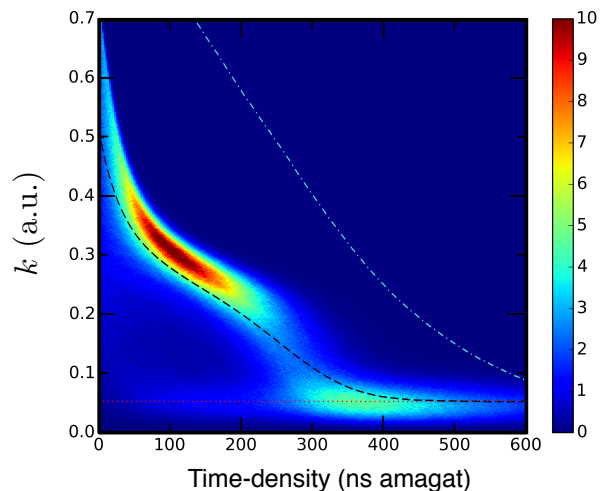


FIG. 3. Density plot of positron momentum distribution $f(k, \tau)$ for Ar, normalised as $\int f(k, \tau) dk = F(\tau)$, the fraction of positrons surviving (dashed-dotted line), calculated using 50,000 positrons initially distributed uniformly in energy up to the Ps-formation threshold. Also shown is the r.m.s. momentum (black dashed line) and thermal momentum $k_{\text{th}} = \sqrt{3k_{\text{B}}T} \sim 0.0528$ a.u. at $T = 293$ K (dotted line).

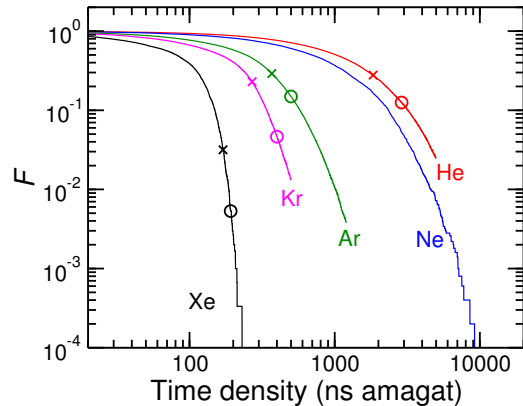


FIG. 4. Calculated fraction of positrons remaining vs. time-density. Crosses indicate the Z_{eff} shoulder lengths (defined in the text); circles indicate the time-density of complete thermalisation, at which the r.m.s. momentum of the distribution k_{rms} is within 1% of $k_{\text{RT}} = \sqrt{3k_{\text{B}}T} \sim 0.0527$ a.u., the momentum of a positron in thermal equilibrium at 293 K.

is within 1% of $k_{\text{th}} \sim \sqrt{3k_{\text{B}}T}$, the r.m.s. for a Maxwell-Boltzmann distribution at 293 K. The values of τ_{th} are marked in Fig. 4, and are presented in Table I, alongside the fractions of initial positrons remaining at that time-density $F(\tau_{\text{th}})$. This fraction is a mere $F(\tau_{\text{th}}) = 0.11$ for helium, and reduces by more than an order of magnitude for xenon. Perhaps most remarkably, the fraction of positrons surviving to thermalization in Ne is zero. This is despite the weak momentum dependence and small

TABLE I. Complete thermalization time-density τ_{th} and \bar{Z}_{eff} shoulder lengths τ_s (both defined in the text) in units of ns amagat, and fraction F of positrons remaining at those times.

	He	Ne	Ar	Kr	Xe
$\tau_{\text{th}}^{\text{a}}$	2890±30	21000±50	500±5	400±10	192±10
$\tau_{\text{th}}^{\text{b}}$	3035±30	23000 ± 500	505±5	460±10	240±10
τ_s^{a}	1839	12075	369	270	170±15
τ_s^{b}	1885	12300	382	440±50	185±20
τ_s^{c}	1700 ± 50	2300 ± 200	362 ± 5	296 ± 6	200 ± 20
τ_s^{d}	–	1700±200	–	–	–
τ_s^{e}	–	–	–	325 ± 6	178 ± 3
τ_s^{f}	1878	>5000	311	288	130
τ_s^{g}	1618	–	–	–	–
$F(\tau_{\text{th}})^{\text{a}}$	0.11	0.00	0.15	0.046	0.0069
$F(\tau_s)^{\text{a}}$	0.28	0.00	0.29	0.23	0.0310

^a This work, initial uniform energy distribution, including depletion of particles due to annihilation, except for Ne and Xe, for which the distribution calculated neglecting annihilation was used.

^b This work, initial positron energies equal to the positronium-formation threshold energy, including depletion of particles due to annihilation, except for Ne and Xe, for which the distribution calculated neglecting annihilation was used.

^c Experiment of Coleman *et al.* [16].

^d Experiment of Coleman *et al.*, determined via intersection of straight line fits to the lifetime spectra [16].

^e Experiment of Wright *et al.* [19].

^f Fokker-Planck calculation of Campeanu and Humberston [29], and Campeanu [20, 21] using polarised-orbital cross sections of McEachran [32–36].

^g Diffusion equation calculation using model potential and enhancement-factor modified zeroth-order annihilation rate [31].

magnitude of $Z_{\text{eff}}(k) \sim 6$ and the similarity of the cross sections to those of helium [40]. In neon, cooling effectively stalls in this minimum (see Fig. 1), with positrons eventually succumbing to annihilation before they can cool further.

Comparison with experiment: time-varying annihilation rate parameter \bar{Z}_{eff} .

Figure 5 shows $\bar{Z}_{\text{eff}}(\tau)$ calculated from the distributions that exclude and include particle loss due to annihilation, for positrons initially distributed uniformly in energy, and with initial energy equal to the positronium-formation threshold. The latter distribution is unrealistic, but provides an upper limit on the cooling time. For all the noble gases the increase in $Z_{\text{eff}}(k)$ as $k \rightarrow 0$ results in the evolution of $\bar{Z}_{\text{eff}}(\tau)$ through a transient ‘shoulder’ region resulting from epithermal annihilation at $k < k_q^{\text{min}}$ [13–15] towards its steady-state thermal value $\bar{Z}_{\text{eff}} \equiv \int_0^\infty Z_{\text{eff}}(k) f_T(k) dk$, where $f_T(k)$

is the Maxwell-Boltzmann distribution taken at $T = 293$ K. Comparisons between theory and experiment are focussed around the shoulder, which is somewhat insensitive to the initial distribution of the positrons [17, 45] (as a result of the bunching around the minimum in $B(k)$). The traditional measure of the thermalization time in positron-gas studies is the ‘shoulder length’ τ_s , defined via $\bar{Z}_{\text{eff}}(\tau_s) \equiv \bar{Z}_{\text{eff}} - 0.1\Delta\bar{Z}$ where $\Delta\bar{Z} = \bar{Z}_{\text{eff}} - \bar{Z}_{\text{min}}$, and \bar{Z}_{min} is the minimum of $\bar{Z}_{\text{eff}}(\tau)$ [54]. The calculated τ_s are given in Table I along with experimental and previous theoretical results [55]. We now consider the results for each atom in turn, leaving Ne to the end as it is atypical.

Helium:—The calculated $Z_{\text{eff}}(\tau)$ is seen to be insensitive to both the initial distribution and whether depletion of the distribution is included or not. It is known that the MBT slightly underestimates the thermal \bar{Z}_{eff} in He, predicting a value of $\bar{Z}_{\text{eff}}=3.79$ compared with the experimental value of 3.94 [16]. Scaling the calculated $Z_{\text{eff}}(\tau)$ to the long-time steady-state experimental value, we find excellent agreement with experiment around the shoulder region, with the calculated shoulder length $\tau_s = 1839$ ns amg agreeing to within 5% of the experimental value of $\tau_s = 1700 \pm 50$ ns amg. The overall shape and length of the calculated shoulder are in better agreement with experiment than the FP calculation of Campeanu and Humberston [29], who used model cross sections. The recent diffusion-model calculation of Boyle *et al.* [31] is also shown. It relied on a model polarisation potential and a zeroth-order $Z_{\text{eff}}(k)$ scaled by enhancement factors, and positrons of initial energy 0.33 a.u. [31]. It produced $\tau_s = 1618$, which underestimates the experimental value. Overall, there is good agreement between the present calculation, that of Boyle *et al.* and experiment. This complements the excellent agreement between the MBT and variational calculations, and measurements of the elastic scattering cross sections [40].

Argon:—The present calculated $Z_{\text{eff}}(\tau)$ are sensitive to the initial distribution at small times, but the overall cooling times for both distributions are similar. The result is weakly sensitive to whether depletion of the distribution is included or not. The calculated thermal $\bar{Z}_{\text{eff}} = 26.0$ is in close to the value of 26.77 measured by Coleman *et al.* [16]. The calculated shoulder time $\tau_s = 369$ ns amg is in excellent agreement with the measured value of 362 ± 5 ns amg [16], with reasonable overall agreement in the shape of the shoulder. A much smaller shoulder length was measured in the Al Qaradawi experiment, which was suspected to have suffered from the presence of impurities [22]. The present calculations show better agreement with experiment than the FP calculation of Campeanu [20], which used the polarized-orbital cross section [35].

Krypton:—The calculated shoulder length and \bar{Z}_{eff} are in excellent agreement with experiment of Wright *et al.* [19] (fluctuations at long times are a result of the small number of positrons remaining). The FP calcula-

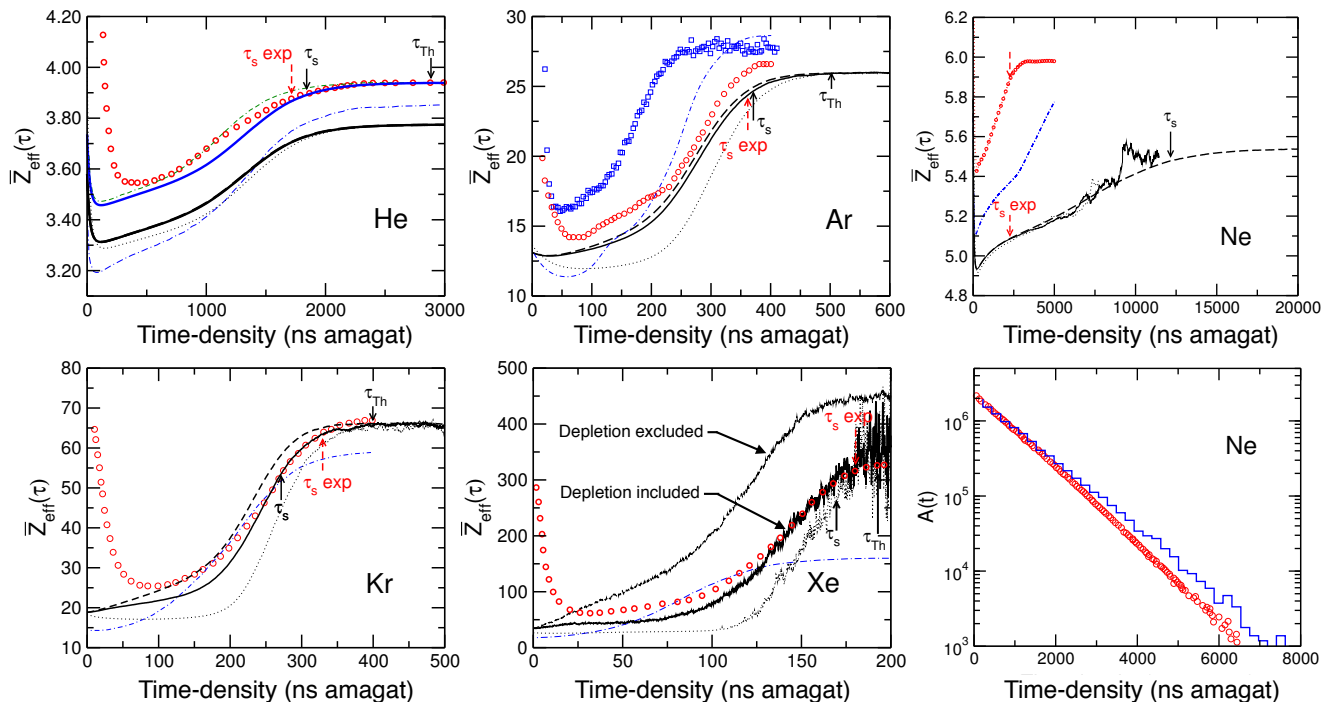


FIG. 5. $\bar{Z}_{\text{eff}}(\tau)$ for He–Xe calculated using $f(k, \tau)$ excluding and including loss of particles due to annihilation, initially distributed uniformly in energy (dashed and solid lines, respectively), and including annihilation with initial energy equal to the Ps-formation threshold (dotted line). Also shown for He: experiment of Coleman *et al.* [16] (red circles), present calculation with \bar{Z}_{eff} scaled to the measured value of $\bar{Z}_{\text{eff}}=3.94$ (blue solid line), FP calculation of Campeanu [29] (blue dashed-dotted line) and model calculations of Boyle *et al.* [31] scaled to $\bar{Z}_{\text{eff}} = 3.94$ (green dash-dash-dotted line); Ar: experiment of Coleman *et al.* [16, 20] (red circles) and Al Qaradawi *et al.* [22] (blue squares), and FP calculation of Campeanu [20]; Kr and Xe: experiment of Wright *et al.* [19] (red circles) and FP calculations of Campeanu [29] (blue dashed-dotted lines); Ne: experiment of Coleman *et al.* [16] (red circles) and FP calculation of Campeanu [29] (blue dashed-dotted lines). The calculated lifetime spectrum [i.e., observed annihilation rate $A(\tau) = -dF(\tau)/d\tau$] for Ne (blue staircase) is also shown (in arbitrary units), compared with experiment [16] (red circles). Arrows mark the calculated (black) and experimental shoulder lengths (red) τ_s .

tion of Campeanu [21], which used the polarized-orbital cross sections [36], underestimates \bar{Z}_{eff} .

Xenon:—The case of Xe is special, because of the large thermal \bar{Z}_{eff} , which means that annihilation successfully competes with cooling at epithermal positron momenta. When positron depletion due to annihilation is neglected, the positron cooling is fast ($\tau_s \sim 150$ ns amg), and Z_{eff} plateaus at ~ 450 . Including depletion brings the shoulder region and shoulder length into excellent agreement with experiment [19] (fluctuations are the result of the small fraction of particles remaining). The FP calculation of Campeanu is in serious disagreement with experiment and the MBT result. It used the model polarised-orbital cross sections of McEachran [36], which predict elastic scattering cross sections and $Z_{\text{eff}}(k)$ that are systematically smaller than the MBT calculation and experiment [40].

Importantly, the present calculations show that \bar{Z}_{eff} is highly sensitive to the loss of particles due to annihilation. The vigorous increase in $Z_{\text{eff}}(k)$ as $k \rightarrow 0$ leads to a quasi-steady-state distribution whose low-momentum

tail is found to be suppressed relative to the Maxwell-Boltzmann one, and a steady-state annihilation rate $Z_{\text{eff}}(\tau \rightarrow \infty) \sim 350$ that is significantly reduced from the calculated true thermal $\bar{Z}_{\text{eff}} \sim 450$. The present results thus conclusively explain the discrepancy between the gas-cell measurement of $\bar{Z}_{\text{eff}} \sim 320$ of Wright *et al.* [19], and the Penning-Malmberg trap measurement $\bar{Z}_{\text{eff}} \sim 401$ of the Surko group [56], whose setup ensures positrons are well thermalized [57].

The effect of rapid annihilation suppressing the low-momentum part of the distribution is demonstrated further in Fig. 6, which shows $\bar{Z}_{\text{eff}}(\tau)$ calculated using an initial *thermal* distribution that excludes annihilation compared with one that is depleted by annihilation. When depletion is included $Z_{\text{eff}}(\tau)$ rapidly reduces (within ~ 5 ns amg) from the thermal value $Z_{\text{eff}}(\tau) \sim 450$ to $\sim 370 \pm 20$ (fluctuations are due to the small fraction of positrons remaining). Figure 6 shows the corresponding momentum distribution $f(k, \tau)$ at $\tau = 0$ and 10 ns amg (both normalized to unity). The suppression of the low momentum part of the distribution is evident. In

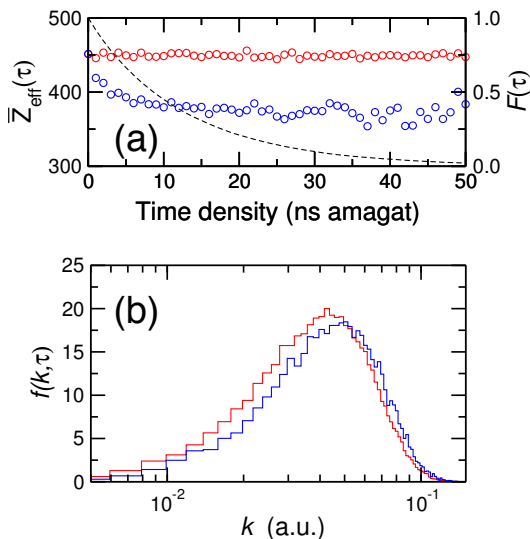


FIG. 6. (a) $\bar{Z}_{\text{eff}}(\tau)$ calculated using an initial thermal distribution of 40,000 positrons, excluding and including depletion of distribution due to annihilation (red and blue circles, respectively). Also shown is the fraction $F(\tau)$ of positrons surviving (dashed line with right axis). (b) the positron momentum distribution (normalized to unity) at $\tau = 0$ (red) and $\tau = 10$ ns amg (blue), calculated with annihilation included.

this case annihilation leads to a heating of the positron distribution.

Neon:—The calculated shoulder time is $\tau_s = 12,000$ ns amg [58], by which time the fraction of positrons remaining is practically zero. It is drastically longer than the measured value $\tau = 2700$ ns amg [16] (note that the FP calculation of Campeanu is also slower and has not reached a steady state value). This serious disagreement is in spite of the good agreement of the MBT elastic scattering cross section with experiment, including at the Ramsauer minimum [40]. Moreover, the present calculation is consistent with that expected from mass scaling the He result $\tau_{\text{th}}^{\text{He}} M_{\text{Ne}}/M_{\text{He}} \sim 5\tau_{\text{th}}^{\text{He}} \sim 14,500$ ns amg.

The experimental shoulder length was determined by Coleman *et al.* [16] via straight line fits to the lifetime spectrum. However, given the serious discrepancy in τ_s , the calculated and measured lifetime spectra are in surprisingly good agreement [see Fig. 5 (f)]. Importantly, the calculated $\tau_s = 12,000$ ns amg and $\tau_{\text{th}} \sim 21,000$ ns amg are much longer than the 0–8000 ns amg considered in the experimental analysis. As seen in Fig. 4, at $\tau \lesssim 8000$ ns amg the vast majority of positrons have already annihilated, after cooling had effectively stalled around the minimum in $B(k)$. Since the $Z_{\text{eff}}(k)$ is a reasonably flat function around the minimum, a signal of many to all of the positrons annihilating at a momenta close to the minimum would be observed as a levelling off of $\bar{Z}_{\text{eff}}(\tau)$, i.e., a characteristic cooling rate measured

over a long time in the lifetime spectra, which could have erroneously been interpreted as the true thermal Z_{eff} . A second possible source of error in the experimental measurement is that it was affected by the presence of impurities. It is known that positron cooling in gases like CO_2 and N_2O is fast, e.g., 0.1 ns amagat [22]. The presence of even minute amounts of impurities could thus lead to a significant reduction in the cooling time.

DISCUSSION

Positron cooling noble gases has been studied using Monte-Carlo simulations based on accurate cross sections calculated *ab initio* from many-body theory. The fraction of positrons surviving annihilation to thermalization has been shown to be strikingly small. For Xe, the time-varying dimensionless annihilation rate $\bar{Z}_{\text{eff}}(\tau)$ is shown to be strongly affected by the depletion positrons due to annihilation. The vigorous increase of the positron annihilation rate as $k \rightarrow 0$ gives rise to a quasi-steady-state distribution whose low-momentum tail is suppressed relative to the Maxwell-Boltzman one. This suppression leads to a reduction in the steady-state \bar{Z}_{eff} , conclusively explaining the long-standing discrepancy between the gas cell and trap-based measurements of \bar{Z}_{eff} . Overall, the use of the accurate atomic data gives the best agreement to date with experiment for all noble gases except Ne, the experiment for which is proffered to have suffered from incomplete knowledge of the fraction of positrons surviving to thermalization and/or the presence of impurities. New experiments of positron cooling in neon are now warranted. Such experiments may include complementary measurements of the time-varying γ spectra during cooling, which have been shown to be sensitive to the positron cooling times [59].

METHODS

Many-body theory calculation of cross sections

Elastic scattering phase shifts and differential and momentum-transfer cross sections

The fully-correlated incident positron *quasiparticle* wavefunction ψ_ε satisfies the Dyson equation (see, e.g., [60, 61]):

$$\left(H_0 + \hat{\Sigma}_\varepsilon\right) \psi_\varepsilon(\mathbf{r}) = \varepsilon \psi_\varepsilon(\mathbf{r}), \quad (3)$$

where H_0 is the unperturbed Hamiltonian of the $N + 1$ particle system, which we take in this work to be the static Hartree-Fock Hamiltonian, and $\hat{\Sigma}_\varepsilon$ is the non-local correlation potential. It is an integral operator that acts as $\hat{\Sigma}_\varepsilon \psi_\varepsilon(\mathbf{r}) \equiv \int \Sigma_\varepsilon(\mathbf{r}, \mathbf{r}') \psi_\varepsilon(\mathbf{r}') d\mathbf{r}'$, and is equivalent to the energy-dependent irreducible self-energy of

the positron in the presence of the atom. Σ is calculated as a diagrammatic expansion, shown in Fig. 7 [37, 51]. Figure 7 (a) describes the polarisation of the atom by the positron, (b) describes the non-perturbative process of virtual-positronium formation, and the third-order diagrams (c)–(g) describe electron screening (see [40, 51] for full details).

The elastic scattering phase shifts δ_ℓ for positrons of angular momenta ℓ can be calculated directly from the corresponding *reducible* self-energy $\tilde{\Sigma}$ as [62]

$$\tan[\Delta\delta_\ell(k)] = -2\pi\langle\varepsilon|\tilde{\Sigma}_\varepsilon|\varepsilon\rangle. \quad (4)$$

where $\delta_\ell(k) = \delta_\ell^{(0)}(k) + \Delta\delta_\ell(k)$ is the total phase shift, with $\delta_\ell^{(0)}$ the static Hartree-Fock field phase shifts, and $\Delta\delta_\ell(k)$ the additional phase shift due to positron-atom correlations described by the self-energy. We use Eqn. 4 to calculate the phase shifts for $\ell = 0, 1$ and 2. The phaseshifts for $\ell > 2$ are accurately described at momenta below the positronium-formation threshold by [63]

$$\delta_\ell(k) \simeq \frac{\pi\alpha_d k^2}{(2\ell - 1)(2\ell + 1)(2\ell + 3)} \quad (\ell \geq 1), \quad (5)$$

where α_d is the dipole-polarisability of the atom.

The differential elastic scattering cross section is determined directly from the scattering phase-shifts via

$$\frac{d\sigma_{\text{el}}}{d\Omega}(\theta, k) = |f(\theta, k)|^2, \quad (6)$$

where σ_{el} is the elastic scattering cross-section, $d\Omega = 2\pi \sin\theta d\theta$ is the solid angle of scattering, and the scattering amplitude is (making use of Eqn. 5)

$$f(\theta) = \sum_{\ell=0}^{\ell_{\text{max}}} (2\ell + 1) \left[\frac{e^{2i\delta_\ell} - 1}{2ik} - \frac{\pi\alpha_d k}{(2\ell - 1)(2\ell + 1)(2\ell + 3)} \right] \\ \times P_\ell(\cos\theta) - \frac{\pi\alpha_d k}{2} \sin\frac{\theta}{2}. \quad (7)$$

The phase shifts are calculated in steps of $\Delta k = 0.02$ a.u. from $k = 0.02$ a.u. up to the Ps-formation threshold, with quadratic interpolation used to determine values between these points. The zero-momentum values are $d\sigma/d\Omega = a^2$ and $\sigma_{\text{el}} = 4\pi a^2$, where a is the scattering length that is calculated from fits of the MBT calculated phase shifts (see Table I in [40]).

The momentum-transfer cross section, defined as [48] $\sigma_{\text{MT}} \equiv \int (1 - \cos\theta) d\sigma/d\Omega d\Omega$, can also be calculated directly from the phase shifts as $\sigma_{\text{MT}} = 4\pi k^{-2} \sum_{\ell=0}^{\infty} (\ell + 1) \sin^2(\delta_{\ell+1} - \delta_\ell)$ (see Fig. 1).

Calculation of the effective annihilation rate $Z_{\text{eff}}(k)$

The rate of positron annihilation on many-electron targets is parametrised Z_{eff} [49, 50]

$$\lambda = \lambda_D Z_{\text{eff}}, \quad (8)$$

where $\lambda_D = \pi r_0^2 c$ is the free-positron (‘Dirac’) rate, where r_0 is the classical electron radius, c is the speed of light, and Z_{eff} is the effective number of electrons that contribute to the annihilation process. The corresponding cross section for positron annihilation in a gas of number density n_g is

$$\sigma_a = \pi r_0^2 n_g \frac{c}{v_r} Z_{\text{eff}}, \quad (9)$$

where v_r is the relative velocity of the positron and electron. Z_{eff} is the effective electron density at the positron

$$Z_{\text{eff}} = \int \sum_{i=1}^Z |\Psi_{\mathbf{k}}(\mathbf{r}_1, \dots, \mathbf{r}_Z; \mathbf{r})|^2 \delta(\mathbf{r} - \mathbf{r}_i) d\mathbf{r}_1 \cdots d\mathbf{r}_Z d\mathbf{r}, \quad (10)$$

where $\Psi_{\mathbf{k}}(\mathbf{r}_1, \dots, \mathbf{r}_Z; \mathbf{r})$ is the total wavefunction that describes the electron and positron system, $\{\mathbf{r}_1, \dots, \mathbf{r}_Z\}$ label the electron coordinates, and \mathbf{r} the positron coordinate. This quantity is both non-local and positron energy dependent. It has the form of an amplitude, with the electron-positron delta function acting as a perturbation. Hence, it is possible to derive a diagrammatic expansion for Z_{eff} [37, 51]. It is shown in Fig. 8. Corresponding algebraic expressions for these diagrams can be found in Refs. [40, 51]. The simplest, zeroth-order diagram [Fig. 8 (a)] corresponds to

$$Z_{\text{eff}}^{(0)} = \sum_{n=1}^Z \int |\phi_n(\mathbf{r})|^2 |\psi_\varepsilon(\mathbf{r})|^2 d\mathbf{r}, \quad (11)$$

i.e., the overlap of the electron and positron densities (n being the n th-electron HF ground-state orbital). It gives Z_{eff} in the independent-particle approximation. Diagrams (a)–(f) provide a complete description of Z_{eff} for one-electron systems, such as hydrogen [51] and hydrogenlike ions [41]. For the many-electron systems considered here, it is also important to account for electron screening in the calculation of Z_{eff} . A series of annihilation diagrams with two Coulomb interactions, similar to the self-energy corrections in Fig. 7 are also included (g)–(m). For full details see [40, 51]. In this work the contribution to the total Z_{eff} due to positron annihilation on valence n subshells of the noble gases, e.g., 5s and 5p subshells in Xe, is calculated including s, p and d-waves including all diagrams (a)–(m). The rate of positron annihilation on core subshells is heavily suppressed due to inability of the positron to overcome the repulsive positron-nuclear potential and penetrate close to the nucleus. However, for the heavier atoms, annihilation on the $(n - 1)$ core subshells can contribute at the $\sim 5\%$ level [40]. We therefore also include the contribution of positron annihilation on the $(n - 1)$ core subshells, e.g., 4s, 4p and 4d subshells in Xe, which were calculated from the expansion of the annihilation amplitude [39, 59, 64], corresponding exactly to diagrams (a)–(f).

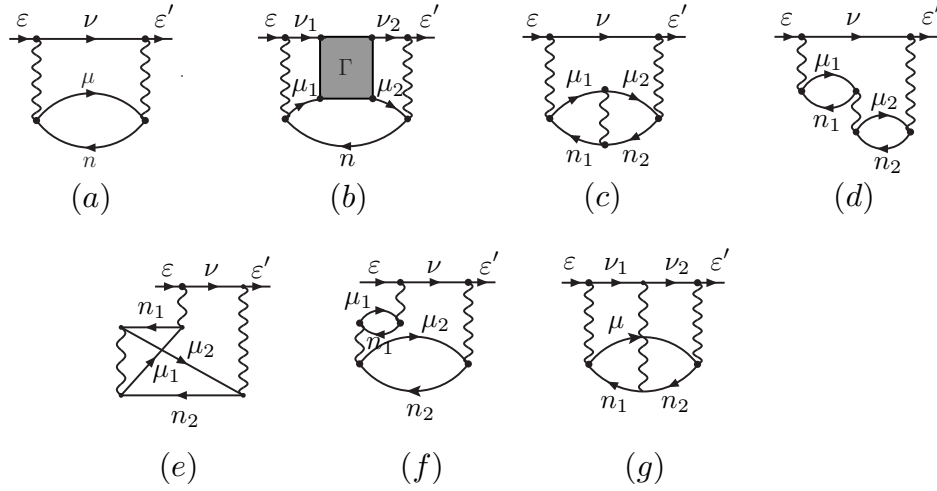


FIG. 7. Diagrammatic expansion of the positron-atom correlation potential (irreducible self-energy of the positron in the field of the atom). Incident and outgoing positron wavefunctions are labelled ε . Single horizontal lines labelled ν represent the propagators for excited positrons in the field of the atom, and lines labelled μ and ν represent propagators for excited electron and hole states, respectively. The shaded Γ block represents the infinite ladder series of excited positron-electron interactions and describes the non-perturbative process of virtual-positronium formation. Summation over all intermediate states is assumed.

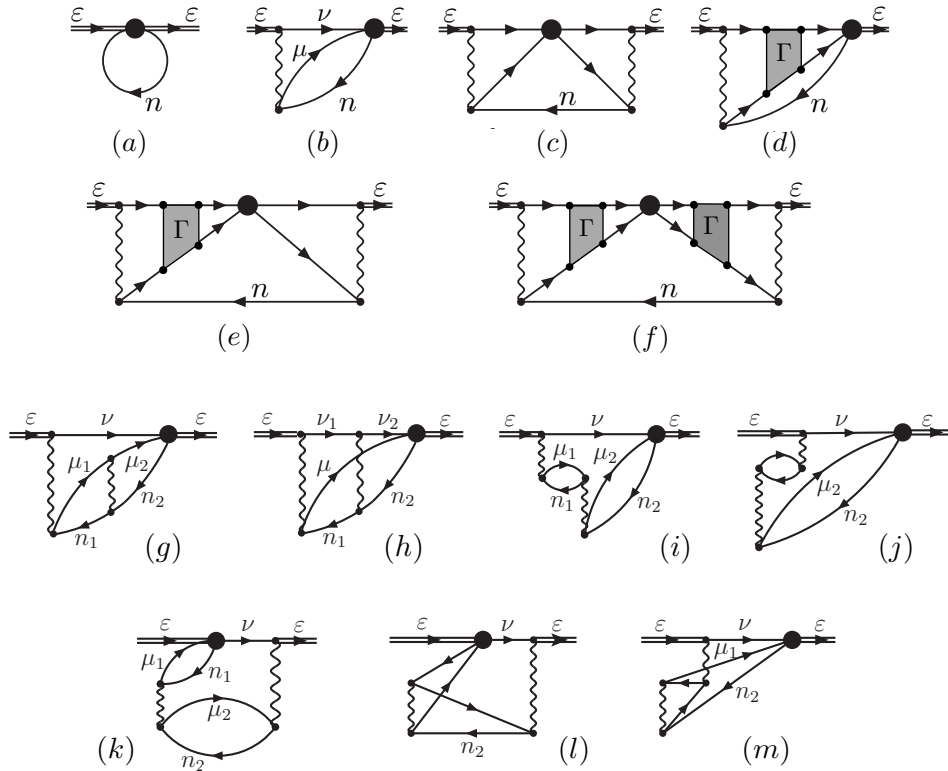


FIG. 8. Diagrammatic expansion of the effective annihilation rate parameter $Z_{\text{eff}}(k)$. In all diagrams the external double lines represent ‘dressed’, positron (Dyson) wavefunction [which involves the sum of all diagrams Fig. (7)], single horizontal lines labelled ν represent the propagators for excited positrons in the field of the atom, and lines labelled μ and ν represent propagators for excited electron and hole states, respectively. The shaded Γ block represents the infinite ladder series of excited positron-electron interactions and describes the non-perturbative process of virtual-positronium formation. Summation over all intermediate states is assumed.

Figure 2 shows the calculated Z_{eff} for the noble gas sequence He–Xe. At zeroth order $Z_{\text{eff}}(k) \propto k^{2\ell}$ as $k \rightarrow 0$, where ℓ is the angular momentum of the positron. Thus s wave annihilation dominates at small momenta, but the contributions from p and d waves become increasingly significant as k increases, leading to the presence of minima. Note the increasingly vigorous momentum dependence at small momenta. At small momenta Z_{eff} can be described analytically as $Z_{\text{eff}}(K) \propto K/(\kappa^2 + k^2) + A$ [37, 38, 65, 66], where K and A are constants and $\kappa = 1/a$ is the reciprocal of the scattering length. The first term is due to the s-wave contribution enhanced by the virtual level (i.e., small $\kappa = 1/a$, $|\kappa| \ll 1/R_a \sim 1$, where R_a is the atomic radius). The constant term A accounts for nonresonant background and contributions of higher partial waves to Z_{eff} . Motivated by this, in this work we parameterize Z_{eff} across the full range of momentum through the Pade approximants

$$Z_{\text{eff}}(k) = \frac{\sum_{n=0}^N b_n k^n}{\kappa^2 + k^2 + \sum_{m=3}^M c_m k^m}, \quad (12)$$

where b_m and c_m are constant coefficients determined from a fit to the true Z_{eff} , and terms up to $M, N \leq 7$ are included to improve the accuracy of the fit. The values of b and c are given in Table II.

TABLE II. Values of constants b and c in Pade approximant for Z_{eff} [Eqn. 12] Number in square brackets denotes multiplication by that many powers of ten.

	He	Ne	Ar	Kr	Xe
b_0	2.015[1]	2.581[1]	1.483	9.535[-1]	7.198[-1]
b_1	-4.594	-7.752	4.711[1]	4.862	-1.900[2]
b_2	2.301[1]	2.455[1]	2.389[4]	2.041[3]	8.599[3]
b_3	-3.924[1]	-6.000[1]	-1.297[5]	-8.501[3]	-8.051[4]
b_4	4.341[1]	6.038[1]	5.399[5]	0.0	4.135[5]
b_5	-2.574[1]	0.0	-4.952[5]	2.691[5]	-7.237[5]
b_6	6.337	0.0	0.0	3.141[5]	5.0448[5]
b_7	0.0	0.0	0.0	0.0	0.0
c_3	2.062	-7.230[1]	1.239[3]	3.977[1]	-2.379[-1]
c_4	-5.902[-1]	4.103[1]	-3.696[3]	0.0	1.227[2]
c_5	0.0	9.507[1]	3.953[4]	-1.021[3]	1.136[3]
c_6	0.0	0.0	-4.362[4]	1.595[4]	0.0
c_7	0.0	0.0	0.0	-1.807[4]	0.0

Monte-Carlo simulation of positron cooling and annihilation

The momentum $k(\tau_i)$ of an individual positron is determined over an equidistant grid in time-density $\{\tau_i\}$ with step size $\Delta\tau$ as follows. The velocity of a gas particle is sampled from the Maxwell-Boltzmann distribution at 293 K. Both it and the positron velocities are transformed to the centre-of-mass frame, in which the energy available for the collision is $E_{\text{CM}} = \mu v_r^2/2$, where μ is the reduced mass and v_r is the relative speed of the positron and gas particle. A uniformly distributed random number $r_1 = U[0, 1]$, is drawn, and a collision is deemed to occur if $r_1 < P = W\Delta\tau$, where $W = n_g v_r \sigma_{\text{tot}}$ is the probability rate of annihilation or elastic collision, with $\sigma_{\text{tot}} = (\sigma_{\text{el}} + \sigma_{\text{a}})$, subject to the requirement that $P = W\Delta\tau \ll 1$ [67]. If a collision occurs, a second random number $r_2 = U[0, 1]$ is drawn. If $r_2 < \sigma_{\text{a}}/\sigma_{\text{tot}}$ the event is deemed to be annihilation and the particle is removed from the simulation, otherwise it is an elastic collision and the positron velocity is updated as follows. The scattering angle θ is sampled from the differential cross section by finding the root of $r_3 = 2\pi\sigma_{\text{el}}^{-1} \int_0^\theta \varrho \sin\theta' d\theta'$, where $r_3 = U[0, 1]$ and $\varrho = d\sigma/d\Omega$ is the differential elastic scattering cross section. In the centre-of-mass frame elastic scattering is symmetric with respect to the azimuthal angle ϕ , which is thus chosen randomly. The momentum distribution $f(k, \tau)$ results from binning positron momenta at each τ_i .

ACKNOWLEDGEMENTS

I thank Gleb Gribakin for insightful discussions and for encouraging my attention to this problem, and Mike Charlton, Christopher Harvey, Matthew Lee and Patrick Mullan for valuable discussions. This work was supported by the United Kingdom Engineering and Physical Research Council (EPSRC), Fellowship Grant EP/EP/N007948/1.

* Correspondences to: d.green@qub.ac.uk

- [1] R. A. Ferrell, “Theory of positron annihilation in solids,” *Rev. Mod. Phys.* **28**, 308–337 (1956).
- [2] F. Tuomisto and I. Makkonen, “Defect identification in semiconductors with positron annihilation: Experiment and theory,” *Rev. Mod. Phys.* **85**, 1583–1631 (2013).
- [3] C. Hugenschmidt, “Positrons in surface physics,” *Surf. Sci. Rep.* **71**, 547 – 594 (2016).
- [4] R. L. Wahal, *Principles and Practice of Positron Emission Tomography* (Lippincott, Williams and Wilkins, Philadelphia, 2008).
- [5] N. Prantzios, C. Boehm, A. Bykov, R. Diehl, K. Ferrière, N. Guessoum, P. Jean, J. Knoedseder, A. Marcowith, I. Moskalenko, A. Strong, and G. Weidenspointner,

- “The 511 keV emission from positron annihilation in the galaxy,” *Rev. Mod. Phys.* **83**, 1001–1056 (2011).
- [6] S. J. Brawley, S. Armitage, J. Beale, D. E. Leslie, A. I. Williams, and G. Laricchia, “Electron-like scattering of positronium,” *Science* **330**, 789–789 (2010).
- [7] The ALPHA collaboration, “Confinement of antihydrogen for 1,000 seconds,” *Nat Phys* **7**, 558–564 (2011).
- [8] G. Gabrielse, R. Kalra, W. S. Kolthammer, R. McConnell, P. Richerme, D. Grzonka, W. Oelert, T. Seitzick, M. Zielinski, D. W. Fitzakerley, M. C. George, E. A. Hessels, C. H. Storry, M. Weel, A. Müllers, and J. Walz (ATRAP Collaboration), “Trapped antihydrogen in its ground state,” *Phys. Rev. Lett.* **108**, 113002 (2012).
- [9] N. et al. Kuroda, “A source of antihydrogen for in-flight hyperfine spectroscopy,” *Nat. Commun.* **5**, 3089 ((2014)).
- [10] G. F. Gribakin, J. A. Young, and C. M. Surko, “Positron-molecule interactions: Resonant attachment, annihilation, and bound states,” *Rev. Mod. Phys.* **82**, 2557–2607 (2010).
- [11] C. M. Surko, G. F. Gribakin, and S. J. Buckman, “Low-energy positron interactions with atoms and molecules,” *J. Phys. B* **38**, R57 (2005).
- [12] Positron lifetime spectroscopy was pioneered by Shearer and Deutsch [68], resulting in the experimental discovery of positronium [69] and its decays [70].
- [13] W. R. Falk and G. Jones, “Experimental studies of the annihilation of positrons in the noble gases,” *Can. J. Phys.* **42**, 1751–1759 (1964).
- [14] S. J. Tao, J. Bell, and J. H. Green, “Fine structure in the delayed coincidence lifetime curves for positrons in argon,” *Proc. Phys. Soc.* **83**, 453 (1964).
- [15] D. A. L. Paul, “The velocity-dependent annihilation rate of slow positrons in argon,” *Proc. Phys. Soc.* **84**, 563 (1964).
- [16] P. G. Coleman, T. C. Griffith, G. R. Heyland, and T. L. Killeen, “Positron lifetime spectra for the noble gases,” *J. Phys. B* **8**, 1734 (1975).
- [17] T. C. Griffith and G. R. Heyland, “Experimental aspects of the study of the interaction of low-energy positrons with gases,” *Phys. Rep.* **39**, 169 – 277 (1978).
- [18] M. Charlton, “Experimental studies of positrons scattering in gases,” *Rep. Prog. Phys.* **48**, 737 (1985).
- [19] G. L. Wright, M. Charlton, T. C. Griffith, and G. R. Heyland, “The annihilation of positrons and positronium formation in gaseous Kr and Xe,” *J. Phys. B* **18**, 4327 (1985).
- [20] R. I. Campeanu, “On the theoretical and experimental cross sections for low-energy positron-rare-gas scattering,” *J. Phys. B* **14**, L157 (1981).
- [21] R. I. Campeanu, “Positron diffusion in krypton and xenon,” *Can. J. Phys.* **60**, 615 (1982).
- [22] I. Al-Qaradawi, M. Charlton, I. Borozan, R. Whitehead, and I. Borozan, “Thermalization times of positrons in molecular gases,” *J. Phys. B* **33**, 2725 (2000).
- [23] M. R. Natisin, J. R. Danielson, and C. M. Surko, “Positron cooling by vibrational and rotational excitation of molecular gases,” *J. Phys. B* **47**, 225209 (2014).
- [24] M. R. Natisin, J. R. Danielson, and C. M. Surko, “A cryogenically cooled, ultra-high-energy-resolution, trap-based positron beam,” *Appl. Phys. Lett.* **108**, 024102 (2016).
- [25] M. Natisin, Ph.D. thesis, University of California, San Diego (2016).
- [26] L. D. Carr, D. DeMille, R. V. Krems, and J. Ye, “Cold and ultracold molecules: science, technology and applications,” *New J. Phys.* **11**, 055049 (2009).
- [27] J. Lim, M. D. Frye, J. M. Hutson, and M. R. Tarbutt, “Modeling sympathetic cooling of molecules by ultracold atoms,” *Phys. Rev. A* **92**, 053419 (2015).
- [28] P. H. R. Orth and G. Jones, “Annihilation of positrons in argon ii. theoretical,” *Phys. Rev.* **183**, 16–22 (1969).
- [29] R. I. Campeanu and J. W. Humberston, “Diffusion of positrons in helium gas,” *J. Phys. B* **10**, 239 (1977).
- [30] B. Shizgal and K. Ness, “Thermalisation and annihilation of positrons in helium and neon,” *J. Phys. B* **20**, 847 (1987).
- [31] G. J. Boyle, M. J. E. Casey, R. D. White, and J. Mitroy, “Transport theory for low-energy positron thermalization and annihilation in helium,” *Phys. Rev. A* **89**, 022712 (2014).
- [32] R. P. McEachran, A. G. Ryman, A. D. Stauffer, and D. L. Morgan, “Positron scattering from noble gases,” *J. Phys. B* **10**, 663 (1977).
- [33] R. P. McEachran, D. L. Morgan, A. G. Ryman, and A. D. Stauffer, “Positron scattering from noble gases: corrected results for helium,” *J. Phys. B* **11**, 951 (1978).
- [34] R. P. McEachran, A. G. Ryman, and A. D. Stauffer, “Positron scattering from neon,” *J. Phys. B* **11**, 551 (1978).
- [35] R. P. McEachran, A. G. Ryman, and A. D. Stauffer, “Positron scattering from argon,” *J. Phys. B* **12**, 1031 (1979).
- [36] R. P. McEachran, A. D. Stauffer, and L. E. M. Campbell, “Positron scattering from krypton and xenon,” *J. Phys. B* **13**, 1281 (1980).
- [37] V. A. Dzuba, V. V. Flambaum, W. A. King, B. N. Miller, and O. P. Sushkov, “Interaction between slow positrons and atoms,” *Phys. Scripta* **T46**, 248 (1993).
- [38] V. A. Dzuba, V. V. Flambaum, G. F. Gribakin, and W. A. King, “Many-body calculations of positron scattering and annihilation from noble-gas atoms,” *J. Phys. B* **29**, 3151 (1996).
- [39] D. G. Green and G. F. Gribakin, “ γ spectra and enhancement factors for positron annihilation with core electrons,” *Phys. Rev. Lett.* **114**, 093201 (2015).
- [40] D. G. Green, J. A. Ludlow, and G. F. Gribakin, “Positron scattering and annihilation on noble-gas atoms,” *Phys. Rev. A* **90**, 032712 (2014).
- [41] D. G. Green and G. F. Gribakin, “Positron scattering and annihilation in hydrogenlike ions,” *Phys. Rev. A* **88**, 032708 (2013).
- [42] D. G. Green, S. Saha, F. Wang, G. F. Gribakin, and C. M. Surko, “Effect of positron-atom interactions on the annihilation gamma spectra of molecules,” *New J. Phys.* **14**, 035021 (2012).
- [43] D. G. Green, S. Saha, F. Wang, G. F. Gribakin, and C. M. Surko, “Calculation of gamma spectra for positron annihilation on molecules,” *Mat. Sci. Forum* **666**, 21–24 (2010).
- [44] The many-body theory has also been successfully applied to positron scattering and annihilation on hydrogenlike ions [41] and to study the effect of positron-atom correlations on positron molecule γ spectra [42, 43].
- [45] A. Farazdel and I. R. Epstein, “Monte carlo studies of positrons in matter. method and application to annihilation spectra in helium gas,” *Phys. Rev. A* **16**, 518–524 (1977).

- [46] D. G. Green, “ANTICOOL: Simulations of positron cooling in atomic gases using differential elastic scattering and annihilation cross sections,” [To be submitted to Comp. Phys. Commun.](#) (2017).
- [47] L. D. Landau and E. M. Lifshitz, *Statistical Physics - Course of Theoretical Physics Volume 5* (Pergamon, Oxford, 1980).
- [48] L. D. Landau and E. M. Lifshitz, *Quantum Mechanics (Non-relativistic Theory) - Third Edition - Course of Theoretical Physics Volume 3* (Pergamon, Oxford, 1977).
- [49] P. A. Fraser, *Adv. At. Mol. Phys.* **4**, 63 (1968).
- [50] I. Pomeranchuk, *Zh. Eksp. Teor. Fiz.* **19**, 183 (1949).
- [51] G. F. Gribakin and J. Ludlow, “Many-body theory of positron-atom interactions,” *Phys. Rev. A* **70**, 032720 (2004).
- [52] V. I. Goldanski and Yu. S. Sayasov, “On the resonance annihilation of positrons in collisions with neutral atoms or molecules,” *Phys. Lett.* **13**, 300 (1968).
- [53] Also see Supplemental Material corresponding videos of the evolution of $f(k, \tau)$ for of all the noble gases: <http://www.am.qub.ac.uk/users/dgreen09/coolingvideos.html>.
- [54] D. A. L. Paul and C. Y. Leung, *Can. J. Phys.* **46**, 2779 (1968).
- [55] As noted by Al Qaradawi *et al.*, and by Paul and Leung [54], systematic errors in experiments may outweigh statistical uncertainties in determining τ_s , and the experimental shoulder lengths may be expected to have uncertainties $\sim 10\%$.
- [56] T. J. Murphy and C. M. Surko, “Annihilation of positrons in xenon gas,” *J. Phys. B* **23**, L727 (1990).
- [57] By adding small amounts of a lighter, low- Z_{eff} gas, e.g., He or H₂, to Xe, Wright *et al.* measured an increase of the pure Xe $\bar{Z}_{\text{eff}} \sim 320$ to $\bar{Z}_{\text{eff}} = 400\text{--}450$ [19], which is broadly consistent with the present calculated value and the Surko group measurement. The mechanism for such an increase with an admixture of He is, however, unclear, given that momentum transfer is more effective in Xe as $k \rightarrow 0$ (see Fig. 1).
- [58] In this case the distribution excluding loss of particles due to annihilation must be used.
- [59] D. G. Green, “Positron cooling in noble gases probed via annihilation γ spectra,” [To be submitted to Phys. Rev. Lett.](#) (2017).
- [60] A. A. Abrikosov, L. P. Gorkov, and I. E. Dzyaloshinski, *Methods of Quantum Field Theory in Statistical Physics* (Dover, New York, 1975).
- [61] A. L. Fetter and J. D. Walecka, *Quantum theory of many-particle systems* (Dover, New York, 2003).
- [62] M. Ya Amusia and N. A. Cherepkov, *Case Studies in Atomic Physics* **5**, 47 (1975).
- [63] T. F. O’Malley, L. Spruch, and L. Rosenberg, “Modification of effective-range theory in presence of a long-range (r^{-4}) potential,” *J. Math. Phys.* **2**, 491 (1961).
- [64] D. G. Green and G. F. Gribakin, “Positron annihilation on core and valence electrons,” [arXiv:1502.08045](https://arxiv.org/abs/1502.08045).
- [65] G. F. Gribakin, “Mechanisms of positron annihilation on molecules,” *Phys. Rev. A* **61**, 022720 (2000).
- [66] J. Mitroy and I. A. Ivanov, “Semiempirical model of positron scattering and annihilation,” *Phys. Rev. A* **65**, 042705 (2002).
- [67] In practice we demand that $P = W\Delta t < 0.1$.
- [68] J. W. Shearer and M. Deutsch, *Phys. Rev.* **76**, 462 (1949).
- [69] M. Deutsch, “Evidence for the formation of positronium in gases,” *Phys. Rev.* **82**, 455–456 (1951).
- [70] M. Deutsch, “Three-quantum decay of positronium,” *Phys. Rev.* **83**, 866–867 (1951).